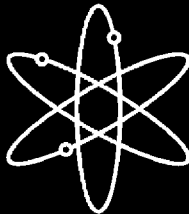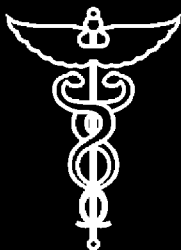# Crack Growth Rates of Irradiated Austenitic Stainless Steel Weld Heat Affected Zone in BWR Environments

Argonne National Laboratory

U.S. Nuclear Regulatory Commission
Office of Nuclear Regulatory Research
Washington, DC 20555-0001

Crack Growth Rates of Irradiated Austenitic Stainless Steel Weld Heat Affected Zone in BWR Environments

Prepared by
O. K. Chopra, B. Alexandreanu, E. E. Gruber,
R. S. Daum, W. J. Shack

Argonne National Laboratory
9700 South Cass Avenue
Argonne, IL 60439

W. H. Cullen, Jr., NRC Project Manager

Abstract

Austenitic stainless steels (SSs) are used extensively as structural alloys in the internal components of reactor pressure vessels because of their superior fracture toughness. However, exposure to high levels of neutron irradiation for extended periods can exacerbate the corrosion fatigue and stress corrosion cracking (SCC) behavior of these steels by affecting the material microchemistry, material microstructure, and water chemistry. Experimental data are presented on crack growth rates (CGRs) of the heat affected zone (HAZ) in Types 304L and 304 SS weld specimens before and after they were irradiated to a fluence of 5.0×10^{20} n/cm^2 (E > 1 MeV) ($\approx$0.75 dpa) at $\approx$288°C. Crack growth tests were conducted under cycling loading and long hold time trapezoidal loading in simulated boiling water reactor (BWR) environments on Type 304L SS HAZ of the H5 weld from the Grand Gulf reactor core shroud and on Type 304 SS HAZ of a laboratory–prepared weld. The effects of material composition, irradiation, and water chemistry on CGRs are discussed.

Foreword

This report examines the effects of simulated light-water reactor coolants, material chemistry, and irradiation damage on crack growth rates (CGRs) in the heat-affected zone (HAZ) of irradiated and nonirradiated, commercially available stainless steels (SSs). This report is one of a series dating back about 8 years, describing such results, which are required to support analysis of the structural integrity of reactor internal components, many of which are subject to irradiation-assisted stress corrosion cracking (IASCC). Earlier publications in this series include NUREG/CR-5608, "Irradiation-Assisted Stress Corrosion Cracking of Model Austenitic Stainless Steels Irradiated in the Halden Reactor"; NUREG/CR-6826, "Fracture Toughness and Crack Growth Rates of Irradiated Austenitic Stainless Steels"; and NUREG/CR-6687, "Irradiation-Assisted Stress Corrosion Cracking of Model Austenitic Stainless Steel Alloys." These earlier reports presented results on specimens irradiated in Phase I (of two) in the Halden test reactor.

This report is the first publication in the series to be built upon specimens irradiated to ~0.75 displacements per atom (dpa) in Phase II in the Halden test reactor. While Phase I irradiations include SSs of wide-ranging chemistry (including commercial steels of typical SS chemistry) and conventional thermomechanical processing, Phase II irradiations include SS weld HAZ materials and several innovatively fabricated and engineered alloys that are designed to be more resistant to IASCC. During the 2006–2008 timeframe, this program will yield publications detailing the results of ongoing and future tests of higher-fluence Phase II irradiations. Irradiation levels in both phases range up to about 3 dpa, making these results most applicable for boiling-water reactor (BWR) internals.

This report presents results with respect to the reference CGR curve presented in NUREG-0313, "Technical Report on Material Selection and Processing Guidelines for BWR Coolant Pressure Boundary Piping," Rev. 2, which the NRC issued in January 1988, for application to intergranular stress corrosion cracking (IGSCC) of pressure boundary piping in BWR plants. The results from the present study show that irradiation, even to the relatively low level of ~0.75 dpa, significantly increases the CGRs in the HAZ of SS welds tested in simulated, normal BWR coolant to values that exceed the NUREG-0313 curve by about a factor of five. The report also shows that thermally treating the nonirradiated materials, to simulate low-temperature sensitization, results in an insignificant change to CGRs in the HAZ. On the positive side, reducing the corrosion potential through testing in simulated hydrogen-water chemistry coolant significantly reduces the CGRs.

_____
Carl J. Paperiello, Director
Office of Nuclear Regulatory Research
U.S. Nuclear Regulatory Commission

Contents

Figures

Tables

Executive Summary

Austenitic stainless steels (SSs) are used extensively as structural alloys in the internal components of reactor pressure vessels (RPVs) because of their relatively high strength, ductility, and fracture toughness. However, exposure to neutron irradiation for extended periods changes the microstructure and degrades the fracture properties of these steels. Irradiation leads to a significant increase in yield strength and reduction in ductility and fracture resistance of austenitic SSs. Also, irradiation exacerbates the corrosion fatigue and stress corrosion cracking (SCC) behavior of SSs by affecting the material microchemistry (e.g., radiation–induced segregation); material microstructure (e.g., radiation hardening); and water chemistry (e.g., radiolysis).

The factors that influence SCC susceptibility of materials include neutron fluence, cold work, corrosion potential, water purity, temperature, and loading. Although a threshold fluence level of 5×10^{20} n/cm^2 (E >1 MeV) (≈ 0.75 dpa) is often assumed for austenitic SSs in the boiling water reactor (BWR) environment, experimental data show increases in susceptibility to intergranular cracking above a fluence of $\approx 2 \times 10^{20}$ n/cm^2 (E >1 MeV) (≈ 0.3 dpa). At low enough fluences, beneficial effects of reducing the corrosion potential of the environment have been observed. However, low corrosion potential does not always provide immunity to irradiation assisted stress corrosion cracking (IASCC), e.g., intergranular SCC has been observed in cold worked, irradiated SS baffle bolts in pressurized water reactors (PWRs).

A program is being conducted at Argonne National Laboratory (ANL) on irradiated SSs to better understand the cracking of BWR internals such as core shrouds. The susceptibility of austenitic SSs to IASCC and the resulting crack growth rates (CGRs) are being evaluated as a function of the fluence level, material composition, and water chemistry. The results from earlier tests in the program on Types 304L and 316L SS irradiated to fluence levels up to 2.0×10^{21} n/cm^2 (E > 1 MeV) (3.0 dpa) indicate significant enhancements in CGRs of irradiated SS in the normal water chemistry (NWC) BWR environment. The observed CGRs of irradiated steels can be a factor of ≈ 5 higher than the disposition curve proposed in NUREG–0313 for sensitized austenitic SSs in water with 8 ppm dissolved oxygen (DO). Type 304L SS irradiated to 3×10^{20} n/cm^2 (0.45 dpa) showed very little environmental enhancement of cyclic CGRs in the NWC BWR environment. In hydrogen water chemistry (HWC) BWR environments, the CGRs of the irradiated steels decreased by an order of magnitude in some tests. The beneficial effect of decreased DO was not observed for a heat of Type 304L SS irradiated to 2×10^{21} n/cm^2, but during that portion of the test, limits on allowable K for irradiated specimens that have been proposed were not met. Thus, the observation may not be valid.

This report presents experimental data on CGRs in the heat–affected zones (HAZs) for several austenitic SS weld specimens that were irradiated to 5×10^{20} n/cm^2 (E > 1 MeV) (≈ 0.75 dpa) at $\approx 288°C$ in a helium environment in the Halden boiling heavy water reactor. The tests were conducted on 1/4–T CT specimens in NWC (300–500 ppb DO) and HWC (≤ 50 ppb DO) BWR environments. The materials were tested under cyclic loading with a triangular or slow/fast sawtooth waveform, and under a trapezoidal waveform with long hold periods. The latter essentially represents constant load with periodic partial unloads. Crack extensions were monitored by direct current (DC) potential drop measurements. The specimens were obtained from Type 304L SS HAZ of the H5 submerged arc (SA) weld of the Grand Gulf (GG) reactor core shroud and Type 304 SS HAZ of a laboratory–prepared shielded metal arc (SMA) weld. They were tested in two conditions: as–welded and as–welded plus thermally treated for 24 h at 500°C. Baseline data were obtained on nonirradiated specimens.

Under loading conditions that result in predominantly mechanical fatigue (i.e., no environmental enhancement), the CGRs for the laboratory–prepared Type 304 SS weld HAZ are consistent with those for austenitic SSs in air, and the rates for the GG Type 304L weld HAZ are a factor of ≈2 lower than those for austenitic SSs in air. Thermal treatment of the material for 24 h at 500°C has little or no effect on mechanical fatigue growth rates.

In the high–DO NWC BWR environment at 289°C at low frequencies (i.e, with environmental enhancement), the cyclic CGRs of Type 304 SS weld HAZ are comparable to those of the GG Type 304L weld HAZ. For the nonirradiated GG and laboratory–prepared weld HAZs, the growth rates in the thermally–treated condition are marginally higher than in the as–welded condition. For both the GG and the laboratory–prepared weld HAZs, irradiation to 5 x 10^{20} n/cm^2 (E > 1 MeV) (≈0.75 dpa) has little or no effect on the cyclic CGRs of the thermally–treated materials, whereas the cyclic CGRs of as–welded materials are increased slightly so that they are comparable to those of the thermally–treated material. In high–DO NWC BWR water, the CGRs for irradiated and nonirradiated thermally–treated HAZ and irradiated as–welded HAZ may be represented by the Shack/Kassner model for nonirradiated austenitic SSs in high–purity water with 8 ppm DO; the rates for nonirradiated as–welded HAZ are slightly lower.

The SCC growth rates are somewhat different from the growth rates under cyclic loading. For the nonirradiated material, limited data suggest that the CGRs for the Type 304 weld HAZ are higher than for the Type 304L weld HAZ. For example, the CGRs of as–welded and as–welded plus thermally–treated GG Type 304L weld HAZ are comparable, and the rates are a factor of ≈2 lower than the NUREG–0313 curve for sensitized SSs in water with 8 ppm DO. The CGR for the thermally–treated Type 304 SS weld HAZ is a factor of ≈10 higher than the CGR for the Type 304L weld HAZ and is a factor of ≈5 higher than the NUREG–0313 curve. CGRs for the as–welded Type 304 SS weld HAZ were not obtained.

The CGRs of all of the SS weld HAZ materials irradiated to 5.0 x 10^{20} n/cm^2 (≈0.75 dpa) are similar and are a factor of 2–5 higher than the NUREG–0313 disposition curve for sensitized SSs in high–DO water. Irradiation increased the CGRs of the as–welded Type 304L weld HAZ, whereas it had little or no effect on the CGRs of the as–welded plus heat–treated Type 304 weld HAZ. A beneficial effect of reducing the corrosion potential of the environment on growth rates was observed for all materials that were tested in both high– and low–DO environments.

The fracture morphology of the Type 304L weld HAZ is somewhat different from that of the Type 304 weld HAZ. For the Type 304 weld HAZ, the morphology was IG under environmentally–enhanced growth conditions or SCC conditions. Transgranular (TG) fracture with a well–defined river pattern was found under conditions that show little or no environmental enhancement. For Type 304L weld HAZ, a TG fracture morphology with a well–defined river pattern was observed under all loading conditions. The fracture morphology for irradiated Type 304 weld HAZ is similar to that of the nonirradiated material.

Acknowledgments

1. Introduction

Austenitic stainless steels (SSs) are used extensively as structural alloys in reactor pressure vessel (RPV) internal components because of their high strength, ductility, and fracture toughness. However, exposure to neutron irradiation for extended periods changes the microstructure and degrades the fracture properties of these steels. Irradiation leads to a significant increase in yield strength and reduction in ductility and fracture resistance of austenitic SSs.[1–4] Radiation can exacerbate the corrosion fatigue and stress corrosion cracking (SCC) behavior of SSs by affecting the material microchemistry (e.g., radiation–induced segregation); material microstructure (e.g., radiation hardening); and water chemistry (e.g., radiolysis).[1,5,6]

The factors that influence SCC susceptibility of materials include neutron fluence, cold work, corrosion potential, water purity, temperature, and loading. The effect of neutron fluence on irradiation–assisted stress corrosion cracking (IASCC) of austenitic SSs has been investigated for boiling water reactor (BWR) control blade sheaths[7–9] and in laboratory tests on BWR–irradiated material[5,10–15]; the extent of intergranular SCC increases with fluence. The percent intergranular (IG) SCC measured in various irradiated austenitic SS specimens is plotted as a function of fast neutron fluence in Fig. 1. Although a threshold fluence level of 5 x 10^{20} n/cm^2 (E >1 MeV) ($\approx$0.75 dpa) has been proposed for austenitic SSs in BWR environments,[5,16] the results in Fig. 1 indicate an increase in IG cracking susceptibility in some commercial–purity SSs at fluence levels above $\approx$2 x 10^{20} n/cm^2 (E >1 MeV) ($\approx$0.3 dpa), and in high–purity heats of SSs at even lower fluence levels.
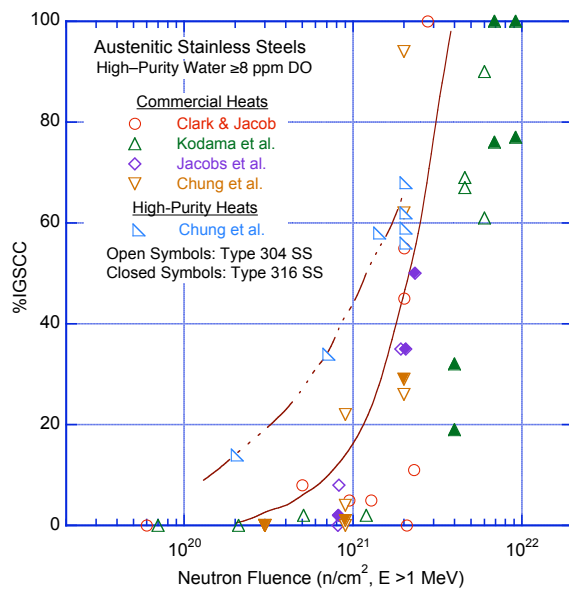
Figure 1.

Susceptibility of irradiated austenitic stainless steels to IGSCC as a function of fluence in high–DO water. From slow–strain–rate tensile tests (Refs. 10,12–14).

Also, constant extension rate tests on Types 304 and 316 SS irradiated to 0.3–4.0 x 10^{21} n/cm^2 (E >1 MeV) in a commercial BWR show a beneficial effect of reducing the corrosion potential of the environment,[17,18] which suggests that the threshold fluence for IASCC will be higher under low potential conditions such as hydrogen water chemistry (HWC) in BWRs or primary water chemistry in pressurized water reactors (PWRs). However, low corrosion potential does not provide immunity to IASCC if the fluence is high enough, e.g., intergranular SCC has been observed in cold–worked, irradiated SS baffle bolts in PWRs.

Argonne National Laboratory (ANL) is conducting a program of SCC testing and associated evaluations on irradiated SSs to support the regulatory request to better understand the safety issues regarding cracking of BWR internals such as core shrouds. The susceptibility of austenitic SSs to IASCC is being evaluated as a function of the fluence level, material composition, and water chemistry. Crack growth rate (CGR) tests are being conducted on Types 304 and 316 SS base metal and weld heat–affected zones (HAZ) irradiated to fluence levels up to 2.0 x 10^{21} n/cm^2 (E > 1 MeV) (3.0 dpa) at ≈288°C. The CGR tests are being conducted in normal water chemistry (NWC) and HWC BWR environments at ≈289°C.

The results of the tests conducted earlier on irradiated Type 304 and 316 SS indicate significant enhancement of CGRs for irradiated steels in the NWC BWR environment.[19,20] Crack growth rates a factor of ≈5 higher than the disposition curve proposed in NUREG–0313[21] for sensitized austenitic SSs in water with 8 ppm dissolved oxygen (DO) have been observed. The CGRs of Type 304L SS irradiated to 0.9 and 2.0 x 10^{21} n/cm^2 (1.35 and 3.0 dpa) and of Type 316L SS irradiated to 2.0 x 10^{21} n/cm^2 (3 dpa) were comparable. A test on Type 304L SS irradiated to 0.3 x 10^{21} n/cm^2 (0.45 dpa) showed little environmental enhancement of cyclic CGRs in the NWC BWR environment, and the CGRs under SCC conditions were below the disposition curve given in NUREG–0313 for sensitized SSs in water with 8 ppm DO.

The results from these earlier tests also indicated that in low–DO BWR environments, the CGRs of the irradiated steels decreased by an order of magnitude in some tests, e.g., Type 304L SS irradiated to 0.9 x 10^{21} n/cm^2 and Type 316L SS irradiated to 2 x 10^{21} n/cm^2. As noted previously, the benefit of low–DO appears to decrease with increasing fluence. A threshold of about 5 x 10^{21} n/cm^2 has been suggested.[5,16] However, the beneficial effect of decreased DO was not observed in a test on Type 304L SS irradiated to 2 x 10^{21} n/cm^2, although it is possible that this different behavior is associated with the loss of constraint in the specimen due to the high applied load.[19]

This report presents experimental data on the CGRs of Types 304L and 304 SS weld HAZ specimens irradiated to ≈5.0 x 10^{20} n/cm^2 (E > 1 MeV) (≈0.75 dpa) at ≈288°C. The irradiations were carried out in a He environment in the Halden heavy water boiling reactor. Crack growth rate tests were performed in BWR environments on Type 304L SS HAZ of the H5 weld from the Grand Gulf (GG) reactor core shroud and on Type 304 SS HAZ of a laboratory–prepared weld. The effects of fluence and water chemistry on growth rates are addressed in this report.

2. Experimental

Crack growth rate tests have been conducted on several austenitic SS weld HAZ specimens that were irradiated to 5 x 10^{20} n/cm^2 (E > 1 MeV) (≈0.75 dpa) at ≈288°C in a helium environment in the Halden boiling heavy water reactor. The tests were performed on 1/4–T compact tension (CT) specimens in NWC and HWC BWR environments at 289°C. Baseline data were obtained on nonirradiated specimens.

2.1 Alloys and Specimen Preparation

A modified configuration of the CT specimen geometry, Fig. 2, was used in the present study. Specimens were obtained from the H5 core–shroud weld of the cancelled GG reactor and a shielded metal arc (SMA) weld prepared from a 30–mm plate of Type 304 SS (Heat 10285). The top and bottom shroud shells for the GG H5 weld were fabricated from SA 240 Type 304L hot–rolled plate using a double–V joint design and welded by the submerged arc (SA) method with ER308L filler metal. The SMA weld was prepared in the laboratory by welding two 70 x 178 mm (2.75 x 7.0 in.) pieces of 30–mm thick (1.18–in. thick) plate. The weld had a single V joint design and was produced by 31 weld passes using E308 filler metal. Passes 1–5 were produced with 3.2–mm (0.125–in.) filler metal rod and 178–mm/min (7–ipm) travel speed, and passes 6–31 were produced with 4.0–mm (0.156–in.) filler metal rod and 216–mm/min (8.5–ipm) travel speed. Between passes the laboratory weld surfaces were cleaned by wire brush and grinding and rinsed with de–mineralized water or alcohol. Similar details of the GG weld preparation are not known to the authors. Because the heat input per pass for SA welds is typically higher than for SMA welds of comparable geometry, the HAZ associated with a SA weld is wider than that associated with a SMA weld.[22,23] However, because the total number of passes are less in a SA weld than in SMA weld, residual strains associated with SA welds are smaller. The composition of Type 304 SSs used in the present study is presented in Table 1.
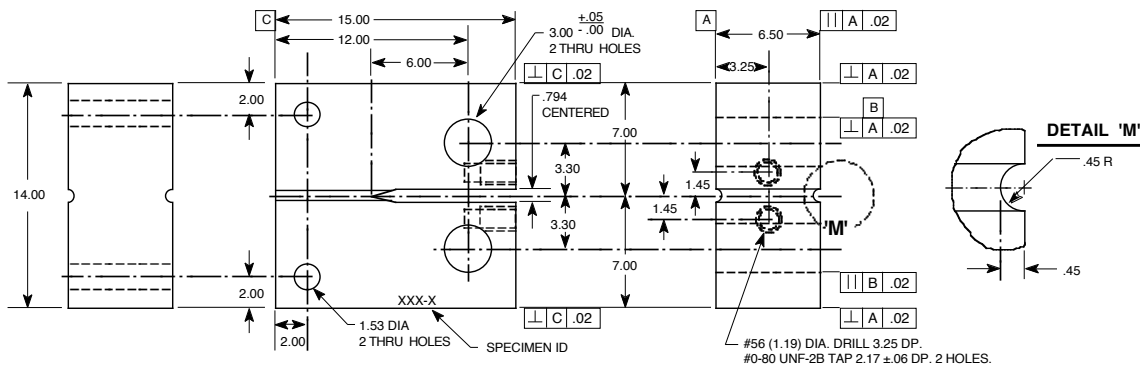
Figure 2.   Configuration of compact–tension specimen used for this study (dimensions in mm).

Table 1.   Composition (wt.%) of Type 304 stainless steels investigated.

Steel Type	Heat ID	Analysis	Ni	Si	P	S	Mn	C	N	Cr	Mo	O
304	10285	Vendor	8.40	0.51	0.032	0.006	1.64	0.058	–	18.25	0.41	–
		ANL	8.45	0.60	0.015	0.007	1.90	0.070	0.084	18.56	0.51	0.013
304L	GG Top Shell	ANL	9.05	0.53	0.027	0.016	1.84	0.013	0.064	18.23	0.44	0.010
	GG Bottom Shell	ANL	8.95	0.55	0.023	0.008	1.80	0.015	0.067	18.62	0.31	0.014

There are two potential differences between the GG SA weld HAZ and laboratory–prepared SMA weld HAZ, e.g., microstructure and residual strain. The HAZ of high–C austenitic SS welds typically consists of a sensitized microstructure. The low–C grades of SSs are considered to be resistant to weld sensitization. A TEM study of the HAZ of the GG Type 304L vertical core shroud weld revealed a few, very small Cr–rich precipitates at the grain boundaries about 1 and 3 mm from the fusion line, most boundaries showed no precipitates.[24] Thus, only the laboratory–prepared weld HAZ is likely to have a sensitized microstructure. The residual strain in various SS weld HAZs have been measured by electron back scattered pattern technique.[24–27] The results indicate that the peak strains typically extend up to 5 mm from the fusion line and range from 8 to 20%. Residual strains up to 10% have been measured in the GG Type 304L vertical core shroud weld HAZ.[24] Similar information for the laboratory–prepared weld HAZ is not available. As discussed earlier, because the total number of passes are greater in SMA than SA welds, residual strain may be greater in HAZs associated with SMA welds of similar geometry.

The specimens were machined from 9.5–mm thick slices of the weld; some slices were thermally treated for 24 h at 500°C to simulate low–temperature sensitization. For all specimens, the machined notch was located in the HAZ of the weld. Each slice was etched, and the specimen orientation and notch location relative to the weld were clearly identified (Figs. 3a, b). In all cases, the machine notch was located ≈1 mm from the fusion zone in a region where the fusion zone was relatively straight. The orientation of the 1/4–T CT specimens obtained from the GG H5 SA weld and laboratory–prepared SMA weld is shown in Figs. 4a and b, respectively.

(a)   (b)
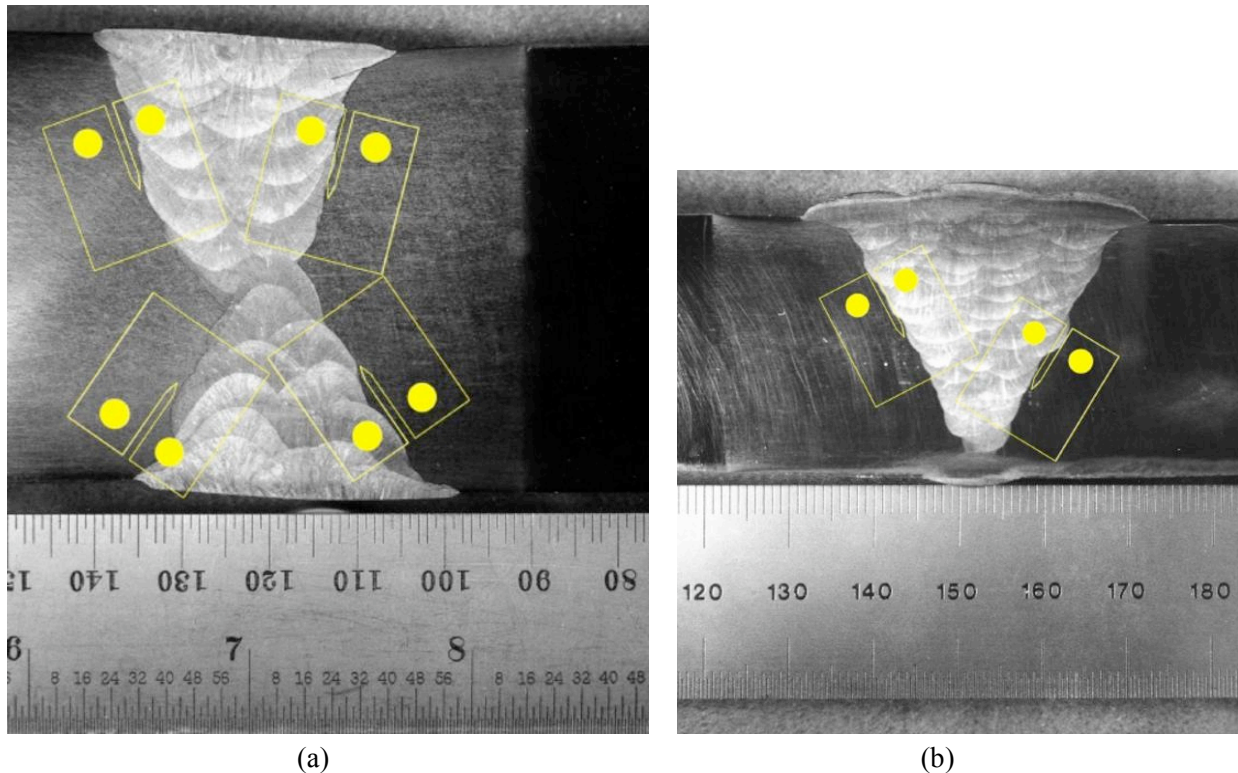
Figure 3. Notch location in the (a) Grand Gulf SA weld HAZ and (b) laboratory–prepared SMA weld HAZ.

4

WELD Slice
Location I.D. (on 4 corners)

Alloy Heat
Identification

~ 8 mm

~ 98 mm

~ 50 mm

(a)

Alloy Heat
Identification

WELD Slice
Location I.D.
(on 2 corners)

~ 143 mm

~ 8 mm

~ 30 mm

(b)
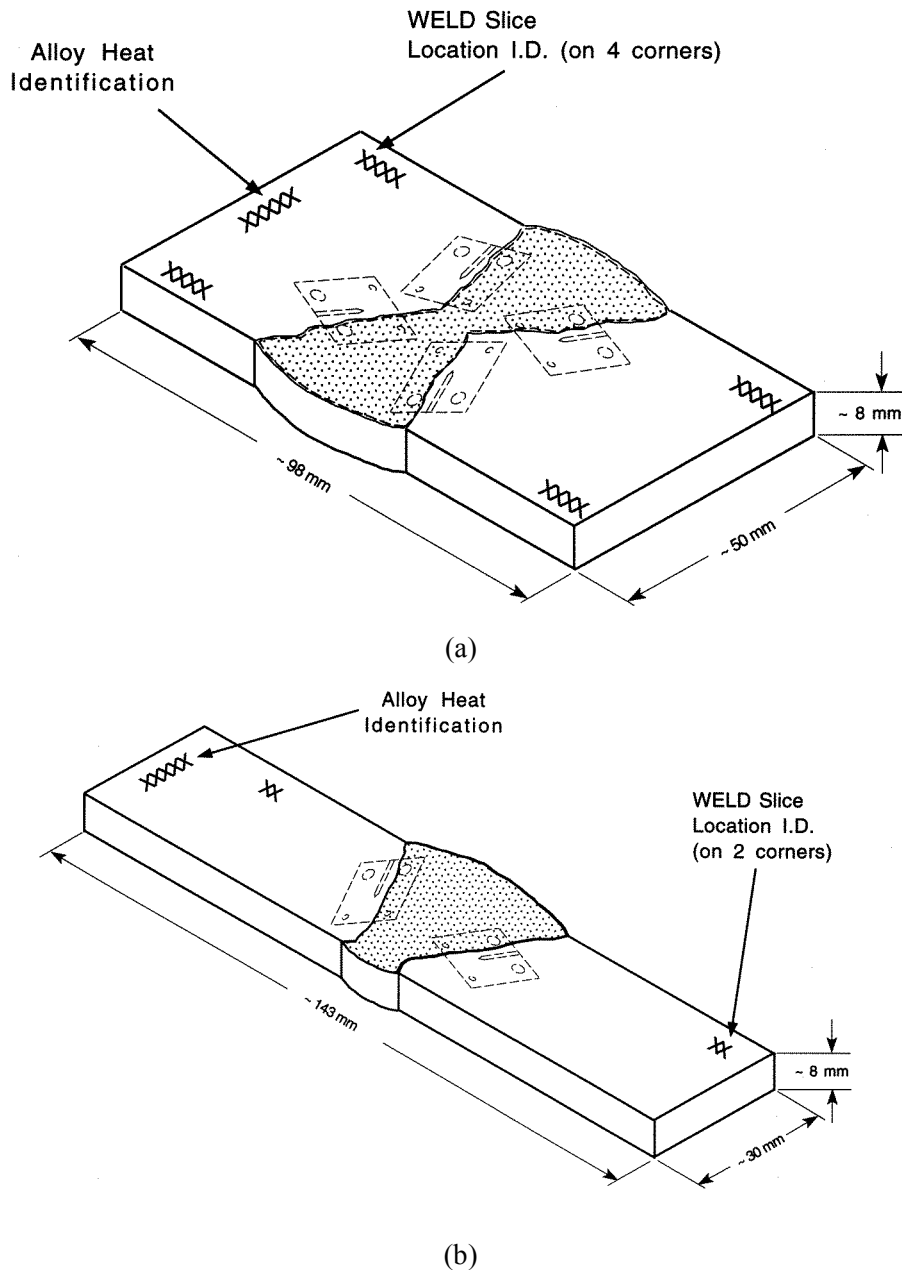
Figure 4. Orientation of the 1/4–T CT specimens from the (a) Grand Gulf H5 SA weld HAZ
and (b) laboratory–prepared SMA weld HAZ.

The microstructures of the base metal and as–welded HAZ of Type 304L SS from the GG top and bottom shells and Heat 10285 of Type 304 SS are shown in Figs. 5–10. The base metal of all the SSs contains stringers of ferrite, e.g., Figs. 5, 7, and 9; Heat 10285 appears to have the most ferrite and the GG bottom shell, the least. The grain sizes for the GG top and bottom shell materials are comparable and are larger than that for Heat 10285, e.g., the grain size in the HAZ region of the GG shell is ≈110 μm and that of Heat 10285 is ≈80 μm. In all welds, the fusion line extends into the base metal along the ferrite stringers, e.g., Figs. 6, 8, and 10. In other words, the ferrite stringers intersecting the fusion line appear to have melted and re–solidified during the welding process.

5
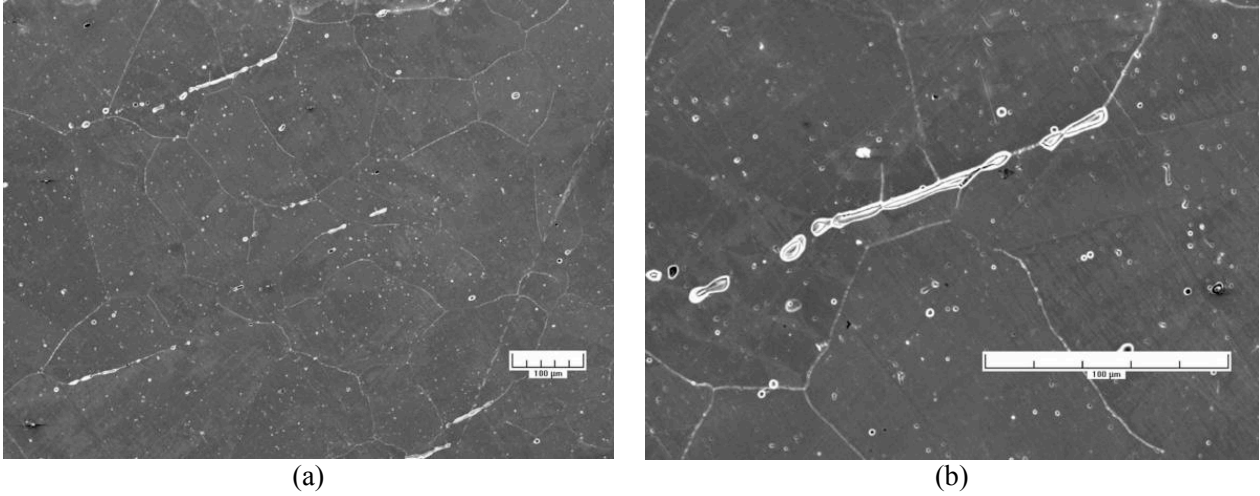
Figure 5. (a) Low- and (b) high–magnification micrographs of the structure of the Type 304L base metal from the top shell of the H5 weld of the Grand Gulf core shroud.
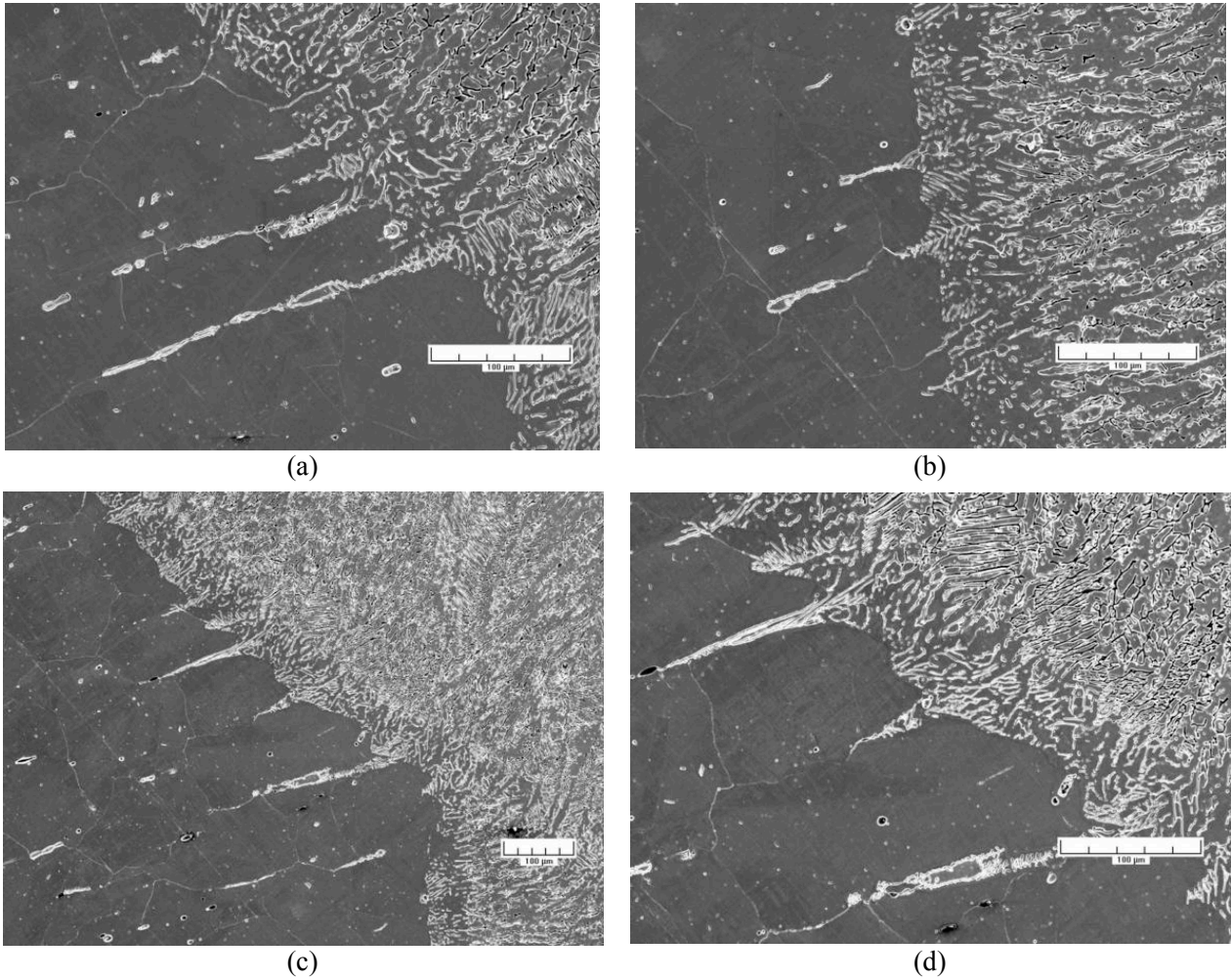
Figure 6. Micrographs of the interface between the weld metal and top shell of the H5 weld of the Grand Gulf core shroud.

(a)   (b)
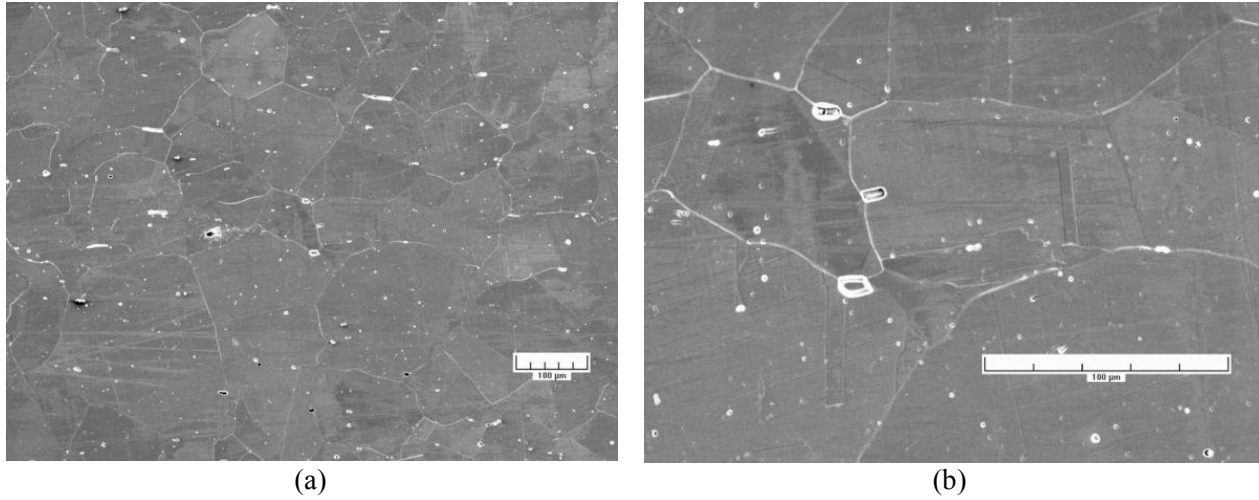
Figure 7.   (a) Low- and (b) high–magnification micrographs of the structure of the Type 304L base
metal from the bottom shell of the H5 weld of the Grand Gulf core shroud.

(a)   (b)

(c)   (d)
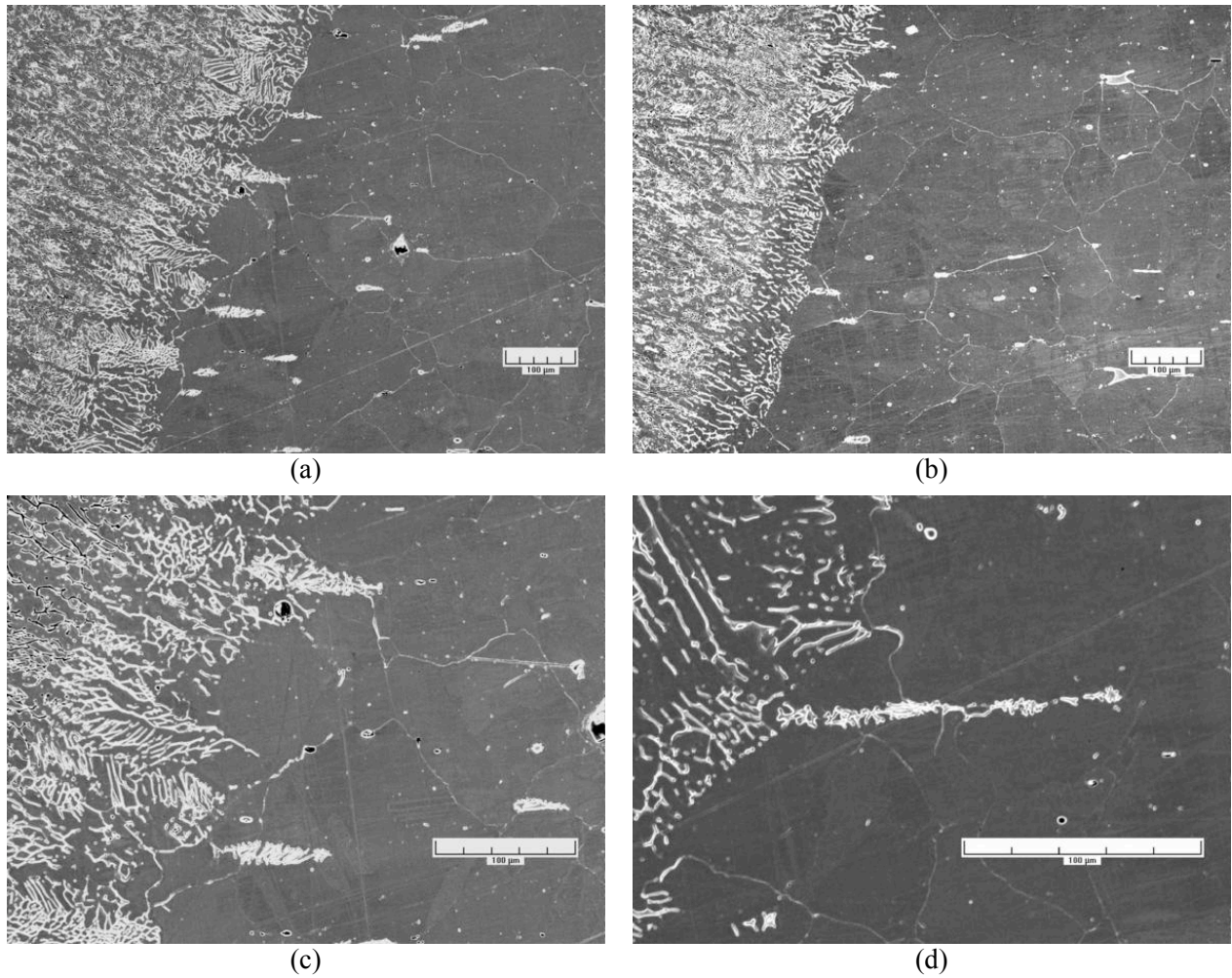
Figure 8.   Micrographs of the interface between the weld metal and bottom shell of the H5 weld of the
Grand Gulf core shroud.

(a)

(b)
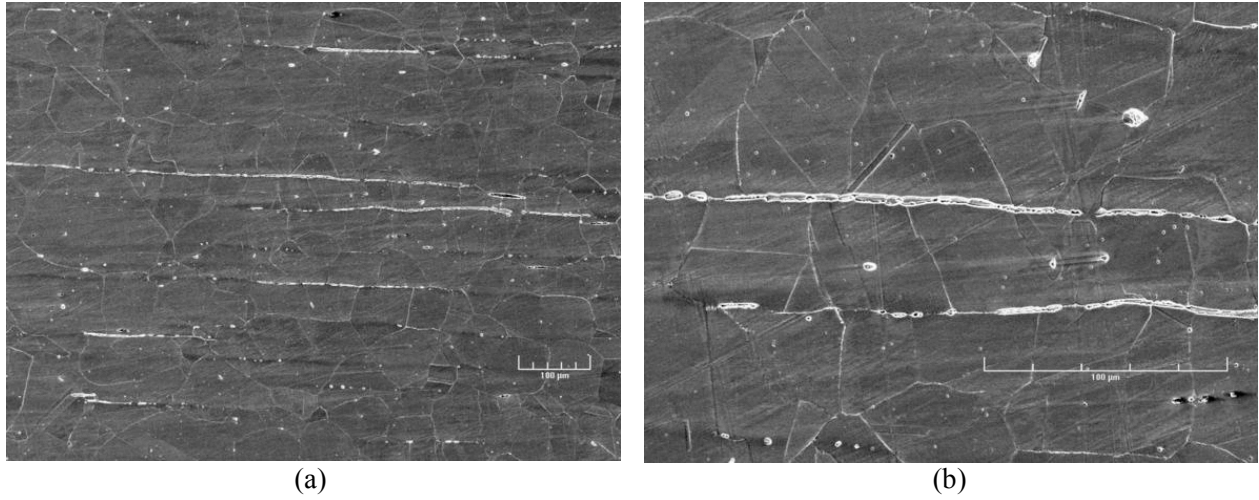
Figure 9.   (a) Low- and (b) high–magnification micrographs of the structure of Heat 10285 of Type 304 stainless steel.

(a)

(b)

(c)

(d)
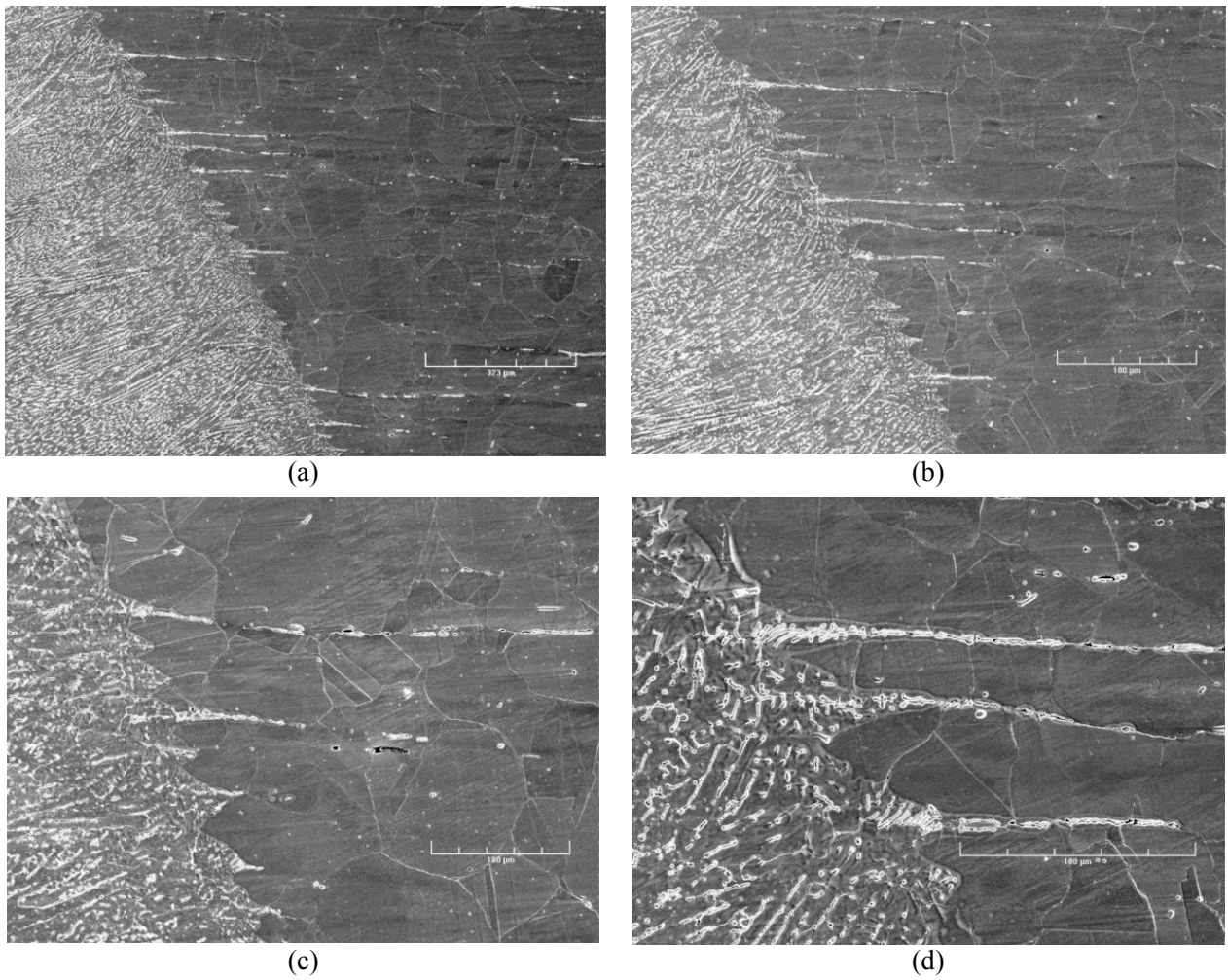
Figure 10.   Micrographs of the interface between the weld metal and base metal of Heat 10285.

The tensile properties of the GG core shroud shell and Heat 10285, in the mill–annealed condition and after sensitization at 600°C for 10.5 h, are listed in Table 2. The tests were conducted on cylindrical specimens, 5.1 mm diameter and 20.3 mm gauge length, in air at 289°C and 0.008 %/s strain rate. The sensitization heat treatment had little effect on the tensile strength of the GG steel, whereas the strength of Heat 10285 was decreased. For the irradiated SSs, the yield stress was estimated from the correlation developed by Odette and Lucas[28]; the increase in yield stress (MPa) is expressed in terms of the fluence (dpa) by the relationship

$$\Delta\sigma_y = 670 \, [1 - \exp(-dpa/2)]^{0.5}. \tag{1}$$

The ultimate stresses for the irradiated steels were estimated from the data in Ref. 14. The tensile yield and ultimate stresses for the irradiated SSs are also given in Table 2. The tensile properties of the sensitized material were used to determine the K/size criterion for nonirradiated and irradiated HAZ specimens, both in the as–welded and as–welded plus thermally–treated conditions.

Table 2.   Tensile properties of the austenitic stainless steels irradiated in the Halden reactor.

Steel Type	Material Condition	Nonirradiated		Fluence 5 x 10^{20} n/cm^2	
		Yield (MPa)	Ultimate (MPa)	Yield (MPa)	Ultimate (MPa)
304 SS Heat 10285	Mill annealed	196	508	–	–
	MA + 10.5 h at 600°C	156	501	531	680
304L SS GG Core Shroud	Mill annealed	158	411	–	–
	MA + 10.5 h at 600°C	159	425	533	610

2.2 Test Facility

The facility for conducting crack growth tests on irradiated materials is designed for in–cell testing, with the test train, furnace, and other required equipment mounted on top of a portable wheeled cart that can be easily rolled into the cell. A 1–liter SS autoclave is installed inside the furnace for conducting tests in simulated BWR environments. Water is circulated through a port in the autoclave cover plate that serves both as inlet and outlet. The hydraulic actuator is mounted on top of the frame, with the load train components suspended beneath it. The 22–kN (5–kip) load cell is at the top of the pull rod. The furnace is mounted on a pneumatic cylinder and can be raised to enclose the autoclave with the load cage and the specimen during the test.

The 1/4–T CT specimen is mounted in the clevises with Inconel pins. The specimen and clevises are kept electrically insulated from the load train by using oxidized Zircaloy pins and mica washers to connect the clevises to the rest of the load train. Platinum wires are used for the current and potential leads. The current leads are attached to SS split pins that are inserted into the holes at the top and bottom of the specimen. The potential leads are attached by screwing short SS pins into threaded holes in the specimen and attaching the platinum wires with in–line SS crimps. An Instron Model 8500+ Dynamic Materials Testing System is used to load the specimen.

The recirculating water system consists of a storage tank, high pressure pump, regenerative heat exchanger, autoclave preheater, test autoclave, electrochemical potential (ECP) cell preheater, ECP cell, regenerative heat exchanger, Mity Mite^{TM} back-pressure regulator, an ion–exchange cartridge, a 0.2 micron filter, a demineralizer resin bed, another 0.2 micron filter, and return line to the tank. A schematic diagram of the recirculating water system is shown in Fig. 11. A detailed description of the test facility is presented in Ref. 19.

9

An out–of–cell test facility, identical to the in–cell test facility but without the ion exchange cartridge (item #28 in Fig, 11), was used to obtain baseline data on nonirradiated specimens. Also, the out–of–cell facility is equipped with a larger feedwater pump that is capable of 30–180 mL/min flow rates, compared to 10–20 mL/min for the in–cell pump.

The BWR environments comprise high–purity deionized water that contains either ≈300 ppb or <30 ppb DO, resulting in ECPs for SS that range from 160 to -500 mV. The feedwater is stored in a 135–L SS tank manufactured by Filpaco Industries.   The tank is designed for vacuums and over–pressures up to 414 kPa (60 psig). The deionized water is prepared by passing purified water through a set of filters that comprise a carbon filter, an Organex–Q filter, two ion exchangers, and a 0.2–mm capsule filter. The DO level in water is established by bubbling nitrogen that contains ≈1% oxygen through the deionized water in the supply tank. For the low–DO tests, the DO level is reduced to <10 ppb by bubbling nitrogen or nitrogen plus 5% hydrogen through the water. The cover gas of the storage tank is nitrogen plus 1% oxygen for the high–DO environment, and either pure nitrogen or nitrogen plus 5% hydrogen for the low–DO environment. The ECP of a Pt electrode and a SS sample located at the exit of the autoclave were monitored continuously during the test, and water samples were taken periodically to measure pH, resistivity, and DO concentration. The DO level was measured in the in–cell facility by the colorimetric technique using CHEMets sampling ampoules and in the out–of–cell facility by a dissolved oxygen analyzer from Orbisphere Laboratories, which included an oxygen indicator and an electrochemical probe.

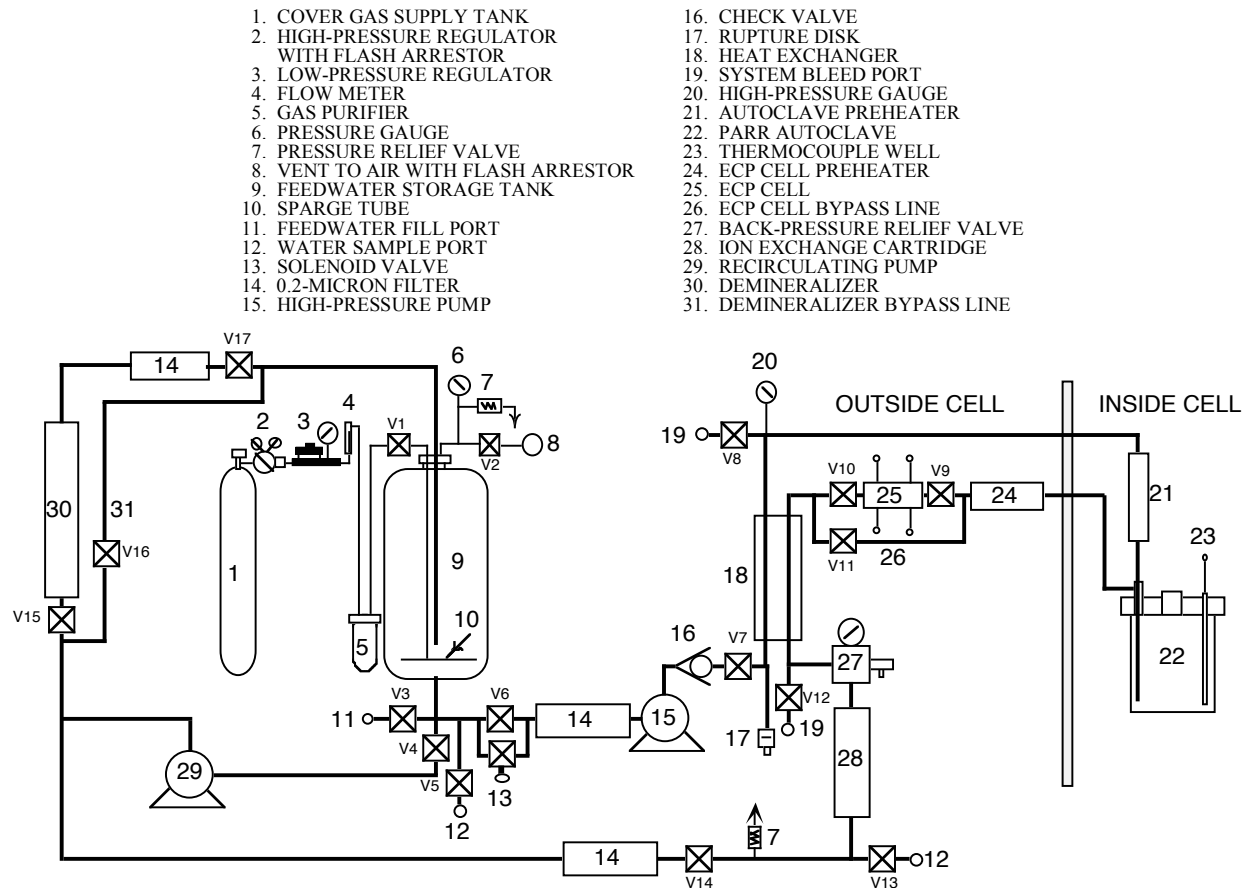|	
1. COVER GAS SUPPLY TANK	16. CHECK VALVE
2. HIGH-PRESSURE REGULATOR WITH FLASH ARRESTOR	17. RUPTURE DISK
	18. HEAT EXCHANGER
3. LOW-PRESSURE REGULATOR	19. SYSTEM BLEED PORT
4. FLOW METER	20. HIGH-PRESSURE GAUGE
5. GAS PURIFIER	21. AUTOCLAVE PREHEATER
6. PRESSURE GAUGE	22. PARR AUTOCLAVE
7. PRESSURE RELIEF VALVE	23. THERMOCOUPLE WELL
8. VENT TO AIR WITH FLASH ARRESTOR	24. ECP CELL PREHEATER
9. FEEDWATER STORAGE TANK	25. ECP CELL
10. SPARGE TUBE	26. ECP CELL BYPASS LINE
11. FEEDWATER FILL PORT	27. BACK-PRESSURE RELIEF VALVE
12. WATER SAMPLE PORT	28. ION EXCHANGE CARTRIDGE
13. SOLENOID VALVE	29. RECIRCULATING PUMP
14. 0.2-MICRON FILTER	30. DEMINERALIZER
15. HIGH-PRESSURE PUMP	31. DEMINERALIZER BYPASS LINE

Figure 11. Schematic diagram of the water system.

2.3 Crack Growth Test Procedure

The CGR tests were performed in accordance with ASTM E–647 "Standard Test Method for Measurement of Fatigue Crack Growth Rates" and ASTM E–1681 "Standard Test Method for Determining a Threshold Stress Intensity Factor for Environment–Assisted Cracking of Metallic Materials under Constant Load."

Crack extensions were determined in–situ by DC potential drop measurements. Because a modified configuration of disc–shaped CT specimen was used in the present study, crack length a, was calculated from the following correlation that was developed from the best fit of the experimental data for normalized crack length and normalized DC potential:

$$\frac{a_i}{W} = \left[0.28887 \left(\frac{U}{U_0} - 0.5 \right) \right]^{0.34775} , \tag{2}$$

where W is the specimen width, and U and U_0 are the current and initial potentials. Equation 2 is comparable to the ASTM E 1737 correlation for a CT specimen with current inputs at the W/4 position and DC potential lead connections at the W/3 position.

The stress intensity factor range ΔK was calculated as follows:

$$\Delta K = \frac{\Delta P}{(BB_N W)^{1/2}} \frac{\left(2 + \frac{a}{W} \right)}{\left(1 - \frac{a}{W} \right)^{3/2}} f\left(\frac{a}{W} \right) \tag{3}$$

$$\Delta P = P_{max} - P_{min} \qquad \text{for R > 0} \tag{4}$$

$$f\left(\frac{a}{W} \right) = 0.886 + 4.64 \left(\frac{a}{W} \right) - 13.32 \left(\frac{a}{W} \right)^2 + 14.72 \left(\frac{a}{W} \right)^3 - 5.6 \left(\frac{a}{W} \right)^4 . \tag{5}$$

where P_{max} and P_{min} are maximum and minimum applied load, a is crack length, and W is the specimen width. The effective thickness B_{eff} of a side–grooved specimen can be calculated as the root mean square of the full and reduced thicknesses, i.e., $(B \cdot B_N)^{0.5}$.

2.2.1 Procedure

All specimens were fatigue precracked in the test environment at load ratio R = 0.2–0.3, frequency of 1–5 Hz, and maximum stress intensity factor $K_{max} \approx 15$ MPa m$^{1/2}$. After 0.3–0.5 mm crack extension, a prescribed loading sequence was followed to facilitate the transition of a TG fatigue crack to a IG stress corrosion crack. To achieve this transition, R was increased incrementally to 0.7, and the loading waveform changed to a slow/fast sawtooth with rise times of 30–1000 s. The loading history was then changed to a trapezoidal waveform, R = 0.7, hold period at peak of 1– or 2–h, and unload/reload period of 24–s to measure SCC growth rates. For some specimens, CGRs were also obtained under constant load. During individual test periods, K_{max} was maintained approximately constant by periodic load shedding (less than 2% decrease in load at any given time).

Under cyclic loading, the CGR (m/s) can be expressed as the superposition of the rate in air (i.e., mechanical fatigue) and the rates due to corrosion fatigue and SCC, given as

$$\dot{a}_{env} = \dot{a}_{air} + \dot{a}_{cf} + \dot{a}_{SCC} . \tag{6}$$

The CGRs in air, $\dot{a}_{air}$ (m/s), were determined from the correlation developed by James and Jones[29]:

$$\dot{a}_{air} = C_{SS}\, S(R)\, \Delta K^{3.3}/T_R , \tag{7}$$

where R is the load ratio (K_{min}/K_{max}), ΔK is $K_{max} - K_{min}$ in MPa m$^{1/2}$, T_R is the rise time (s) of the loading waveform, and function S(R) is expressed in terms of the load ratio R as follows:

$$
\begin{aligned}
S(R) &= 1.0 & R &< 0 \\
S(R) &= 1.0 + 1.8R & 0 &< R < 0.79 \\
S(R) &= -43.35 + 57.97R & 0.79 &< R < 1.0
\end{aligned}
\tag{8}
$$

Function C_{SS} is given by a third–order polynomial of temperature T (°C), expressed as

$$C_{SS} = 1.9142 \times 10^{-12} + 6.7911 \times 10^{-15}\, T - 1.6638 \times 10^{-17}\, T^2 + 3.9616 \times 10^{-20}\, T^3. \tag{9}$$

Environmental effects on fatigue crack growth of nonirradiated austenitic SSs have been investigated by Shack and Kassner.[30] In the absence of any significant contribution of SCC to growth rate, the CGRs in water with ≈0.3 ppm DO are best represented by the expression,

$$\dot{a}_{env} = \dot{a}_{air} + 4.5 \times 10^{-5}\, (\dot{a}_{air})^{0.5} \tag{10}$$

and in water with ≈8 ppm DO by the expression,

$$\dot{a}_{env} = \dot{a}_{air} + 1.5 \times 10^{-4}\, (\dot{a}_{air})^{0.5}. \tag{11}$$

The CGR (m/s) under SCC conditions is represented by the correlation given in NUREG–0313, Rev. 2,[21]

$$\dot{a}_{SCC} = A\,(K)^{2.161}, \tag{12}$$

where K is the stress intensity factor (MPa m$^{0.5}$), and the magnitude of constant A depends on the water chemistry and composition and structure of the steel. A value of 2.1 x 10^{-13} has been proposed in NUREG–0313 for sensitized SS in water chemistries with 8 ppm DO. The magnitude of constant A will be smaller in low–DO environments such as HWC BWR or PWR.

During crack growth tests in high–temperature water, environmental enhancement of CGRs typically does not occur from the start of the test. Under more rapid cyclic loading typically used for precracking, the crack growth is dominated by mechanical fatigue. The CGRs during precracking and initial periods of cyclic loading in these tests were primarily due to mechanical fatigue. For tests under increasing rise times, the CGRs first decrease along the diagonal as shown by the curve denoted "Precracking" in Fig. 12, then jump to new, higher environmentally enhanced growth rates. For K_{max} values of 15–18 MPa m$^{1/2}$, environmental enhancement typically occurred at load ratios R ≥ 0.5 and rise times ≥ 30 s.
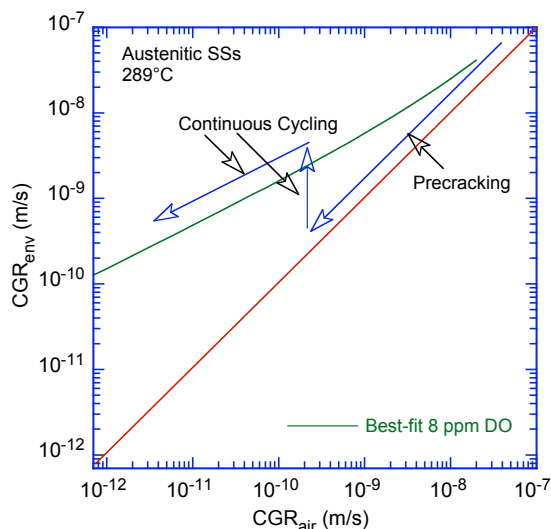
Figure 12.
Plot of CGR in water vs. the CGR in air showing environmental enhancement of growth rates in high purity water at 289°C.

All tests were started in high–purity water that contained 250–500 ppb DO (i.e., NWC BWR environment). The ECPs of a Pt electrode and a SS sample located at the exit of the autoclave were monitored continuously during the test; the water DO level and conductivity were determined periodically. After data were obtained in high–DO water, the DO level in the feedwater was decreased to < 30 ppb by sparging the feedwater with pure N_2, or N_2 + 5% H_2. Because of the very low water flow rates, it took several days for the environmental conditions to stabilize for the in–cell tests. In general, the changes in ECP of the SS sample were slower than those of the Pt electrode. Because of the higher flow rates, the changes in water chemistry for the out–of–cell tests were significantly faster.

After the test the final crack size was marked by fatigue cycling in air at room temperature. The specimens were then fractured, and the fracture surface of both halves of the specimen was photographed with a telephoto lens through the hot cell window. The fracture surfaces of the out–of–cell test specimens were examined by scanning electron microscopy (SEM). The final crack length of each half of the fractured specimen was determined from the optical or SEM photograph by the 9/8 averaging technique, i.e., a total of nine measurements were taken across the width of the specimen at equal intervals, the two near–surface measurements were averaged and the resultant value was averaged with the remaining seven measurements. The results were used to correct the experimental crack length measurements, e.g., the crack extensions determined from the DC potential drop method were proportionately scaled to match the final optically measured crack length.

The CGR during each test period was determined from the slope of the corrected crack length vs. time plots; for cyclic loading, only the rise time was used to determine growth rate. The crack extension during each test period was at least 10 times the resolution of the DC potential drop method, i.e., typically 5 μm. Thus, crack extensions were at least 50 μm; for test periods with very low CGRs, e.g., less than 1 x 10^{-11} m/s, smaller crack extensions were used to reduce testing time. Thus, for both GG SA weld HAZ and laboratory–prepared SMA weld HAZ, the crack extension during most test periods was less than a grain size. Nevertheless, the propagating crack encounters ≈70 and 55 grains across the width of the laboratory–prepared HAZ specimen and GG HAZ specimen, respectively. A simple statistical formalism by Alexandreanu and Was[31] may be used to evaluate how representative are these samples of the material being investigated. Assuming that random boundaries are susceptible to cracking and random boundary fraction is typically 50% in austenitic SSs, the fractional error associated with the cracking–susceptible random boundaries that would result from a sample of 70 or 55 grains is relatively small, e.g., 12 and 14%, respectively.

13

2.2.2 SEM Examination of Fracture Surfaces

The fracture surfaces of the irradiated specimens were also examined by a scanning electron microscope (SEM) located in the hot–cell facility to further validate the crack extension measurements and to characterize the fracture morphology. To reduce the exposure to the SEM operator, the examinations were performed on thin slices of the fracture surface cut from the fractured CT specimen using a Charmilles-Andrew Model EF330 traveling–wire electro–discharge machine (EDM).

Distilled water flows around the EDM cutting wire, forming a dielectric medium between the wire and the CT specimen in order to facilitate the non–contacting erosion of the specimen. A schematic of the EDM cutting facility is shown in Fig. 13. The facility includes a EDM cutting water basin with a primary filter and debris screen, a 15–gal plastic tank to hold the secondary filter bag and the filtered water inside the cell, and a plumbing system consisting of an in–line peristaltic water pump, a valve, and tygon tubing for transferring the filtered water from the 15–gal tank through the cell wall to a waste container. The waste container is placed within a lead–lined 55–gal drum, and the dose rate of the waste–water is continuously monitored from the side of the lead–lined drum. To ensure that the specimen is square to the movement of EDM wire, the CT specimen was kept stationary in a custom–built fixture while the movement of the brass cutting wire (with a zinc-coating for strength and durability) was computer controlled with a precision of 1.3 μm (0.00005 in.) in the horizontal plane.
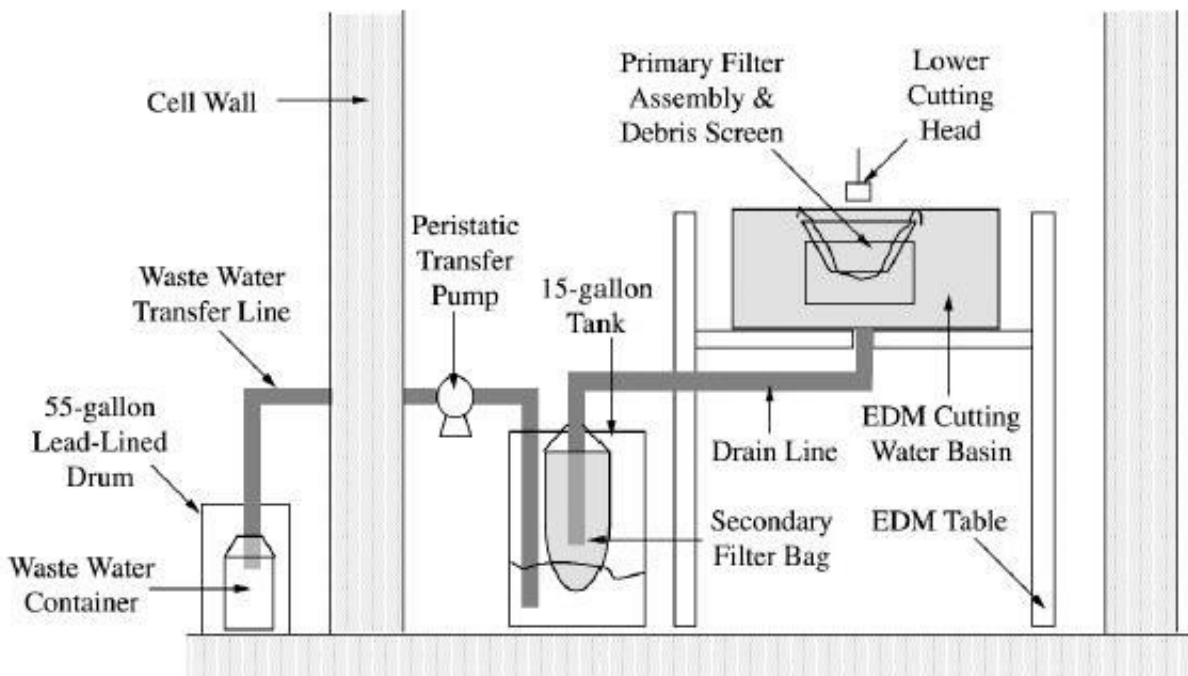

Figure 13.   A schematic of the EDM cutting facility and the waste–water plumbing system.

For a detailed examination of the fracture surfaces, some nonirradiated specimens of interest were stripped of oxides using a two–step procedure. First, the specimens were boiled in a solution consisting of 20% NaOH and 5% KMnOH for 1 h. Then, they were boiled for an additional 1 h in a 20% $(NH_4)_2C_6H_6O_7$ solution. Upon completion of this procedure, the samples were ultrasonically cleaned successively in distilled water, methanol, and isopropanol. None of the fracture surfaces of the irradiated specimens were stripped of oxides.

2.2.3 Data Qualification

The CGR test results were validated in accordance with the specimen size criteria of ASTM E 1681 and E 647. These criteria require that the plastic zone at the tip of a fatigue crack be small relative to the specimen geometry. The ASTM specifications for specimen K/size criteria are intended to ensure applicability and transferability of the cracking behavior of a component or specimen of a given thickness under a specific loading condition to a crack associated with a different geometry, thickness, and loading condition.

For constant load tests, ASTM E 1681 requires that

$$B_{eff} \text{ and } (W - a) \geq 2.5 \, (K/\sigma_{ys})^2, \tag{13}$$

and for cyclic loading ASTM 647 requires that

$$(W - a) \geq (4/\pi) \, (K/\sigma_{ys})^2, \tag{14}$$

where K is the applied stress intensity factor, and σ_{ys} is the yield stress of the material. For tests on irradiated material, side–grooved specimens are strongly recommended, with a depth for each side groove between 5 and 10% of the specimen thickness. In high–temperature water, because the primary mechanism for crack growth during continuous cycling is not mechanical fatigue, Eq. 13 is the more appropriate criterion, but Eq. 14 may give acceptable results. For high–strain hardening materials, i.e., materials with an ultimate–to–yield stress ratio (σ_{ult}/σ_{ys}) ≥ 1.3, both criteria allow the use of the flow stress defined as $\sigma_f = (\sigma_{ult} + \sigma_{ys})/2$ rather than the yield stress.

The K/size criteria were developed for materials that show work hardening and, therefore, may not be valid for materials irradiated to fluence levels where, on a local level, they do not strain harden. This lack of strain hardening, or strain softening, is most dramatic when dislocation channeling occurs but may also occur at lower fluences. For moderate to highly irradiated material, it has been suggested that an effective yield stress, defined as the average of the nonirradiated and irradiated yield stresses, be used[32]. This discounts the irradiation–induced increase in yield stress by a factor of 2. In the present study, because of relatively low fluence level, flow stress was used to determine the valid K_{max} for both nonirradiated and irradiated SS weld HAZ specimens.